

# Advanced Insolation Detection Module in Solar Shading Automation

Robert Weitlaner<sup>1</sup>, David Geisler-Moroder<sup>2</sup>, Rainer Pfluger<sup>3</sup>

<sup>1</sup>HELLA Sonnen- und Wetterschutztechnik GmbH, Abfaltersbach, Austria

<sup>2</sup>Bartenbach GmbH, Aldrans, Austria

<sup>3</sup>Unit for Energy Efficient Building, Leopold Franzens University of Innsbruck, Austria

## Abstract

This work is proposing an approach for controlling solar shading devices under different insolation states solving certain issues of a multisensor network. Disapproval of solar shading automation is caused by false state detection whether a window is not exposed (state 0), directly exposed (state 2) or exposed via specular reflection on nearby structures (state 1). State 1 is never detected by common approaches: A sensor on a roof might detect the sky condition, but cannot provide the current state of each individual window. Multi-sensor networks promise to distinguish between state 0 and 2 based on fuzzy thresholds. Window centered shadow masks for every single window cannot detect state 1. This shortcoming is eliminated by raytracing pre-calculation of the insolation state per time steps. The accuracy of this data was tested on a real case study and the approach will be integrated into building automation by end of 2017.

## Introduction

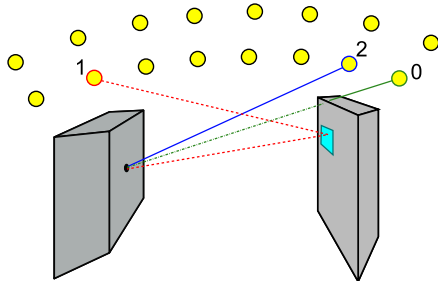


Figure 1: Insolation state definition: shaded (0), insulated via reflection (1), direct (2).

Shading automation for venetian blinds is depending on accurate detection of the insolation state of every individual window. In Figure 1 these states are

- 0 ... shaded
- 1 ... hit via reflection
- 2 ... hit by direct beam.

There are many different control strategies available to control solar gains and visual comfort. For louver systems mainly three operations are common:

1. retract the system,

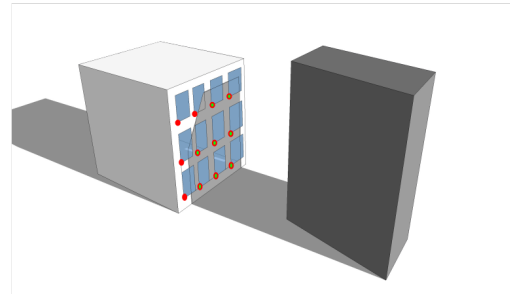


Figure 2: Sensor network detecting insolation.

2. control glare caused by high sky luminance or reflection from adjacent surfaces (static surfaces and movable ones) by rotating to one fixed tilt angle,
3. block direct insolation by *dynamically* tilting according the current sun position (e.g. cut-off control).

There is no difference between operations 2 and 3 for simple fabric roller blinds. Louver systems at a fixed tilt angle of about 45° - for 80mm wide and 72mm spaced louvers - reduce visible average luminances in the field of view. The description of insolation especially for buildings in densely built-up areas such as urban high-rise city districts is cumbersome and cost intensive. Different approaches have been developed, but they all cannot solve the problem comprehensively. Two approaches are shadow masks or multi-sensor networks:

- Shadow masks—per facade or per window—are measured on site or pre-calculated, but cannot provide control of reflected glare.
- A multi-sensor network (Fig. 2) is hypothetically resilient regarding the evolution of neighboring shadowing and movable reflecting structures (e.g. surfaces of cars). But, as shown in Figure 3, the definition of thresholds between states 0, 1 and 2 is fuzzy: An illuminance reading between values **b** and **d** (Figure 3) cannot be clearly attributed to one state as it might result from
  - a low luminance cloudy sky (blue),
  - an intermediate luminance or insolation via reflection (green) or

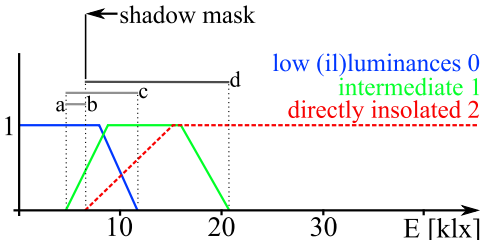


Figure 3: Fuzzy thresholds in solar automation.

- also low angle incident direct insolation (red).

If a sensor reading between **b** and **d** is combined with a shadow mask, the source of direct insolation might be eliminated. Hence, the possible solutions are reduced to 0 and 1, but the correct detection is still impossible.

Figure 4 shows the scheme of our proposed approach, which solves the issues of a multi-sensor network: Thresholds for distinction between direct insolation (state 2) and high luminance skies or reflected illuminances (state 1) are no longer required. They are replaced by well-defined state descriptions per individual test point (e.g. Point A and B) and time step (Figure 5). These values 0,1,2 are collected in a matrix  $S$ , Figure 4.

The main input to the proposed shading control in Figure 4 is delivered by a roof-mounted sensor (Figure 6). The current sky condition is evaluated against the matrix entry before sending positioning commands to the louver actors. The roof-mounted sensor must not be shaded by other buildings, and in future prospects, one single high-quality sensor could deliver data for a complete city district. The detection of a clear sky relies on the ratio diffuse and direct irradiance as in Weitlaner et al. (2013) or delivered from advanced measurement devices as for example the SPN1 global and diffuse pyranometer or even luminescence cameras.

Nowadays, all necessary input data is available in appropriate accuracy for realizing this approach:

- digital elevation models,
- digital city models,
- digital building models.

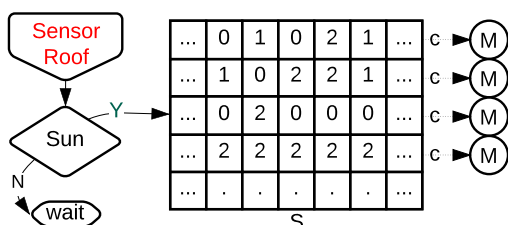


Figure 4: Shading Automation:  $S \dots$ matrix;  $c \dots$ command;  $M \dots$ motor

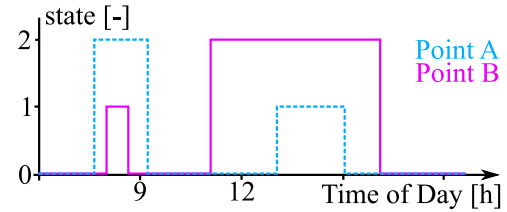


Figure 5: Pointwise defined insolation states over time.

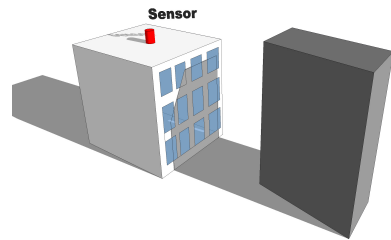


Figure 6: Sun detection with unshaded roof-mounted sensor.

## Simulation

### Annual Daylight Simulations

Annual daylight illuminance ( $E$ ) calculations are based on a matrix approach,

$$E_{i,k} = \sum_{j=1}^{j_{max}} C_{i,j} \cdot s_{j,k} \quad (1)$$

defined by following procedure:

1. define a set of  $n$  target points, index  $i$ ,
2. discretize the sky into sky patches, index  $j$ ,
3. calculate contribution coefficients  $C_{i,j}$ , called daylight coefficients,
4. derive a luminance/radiance  $s_j$  for each sky patch  $j$  and time step  $k$  based on a weather file through a sky model.

The sky discretization  $j_{max}$  is usually based on Tregenza (1987), who defined 151 patches with about 11,4° opening angle. Based on that, the official definition consists of 145 patches in Borisenkov et al. (1994) CIE 1994 and Tab. 1). Reinhart's subdivision

Table 1: Tregenza's 145 Sky Patches; seven rows, height 12°, plus one final one, plus one patch for complete bottom hemisphere.

$\phi$	6	18	30	42	54	66	78	90
#	30	30	24	24	18	12	6	1

of these Tregenza patches in Bourgeois et al. (2008) is available in Radiance's *genskyvec* Ward et al. (2011), where  $j_{max} = 145, 2305$  or 5185.

The number of time steps is theoretically arbitrary but as weather files are available in an hourly resolution,  $k_{max}$  is usually 8760. Thus the dimension of

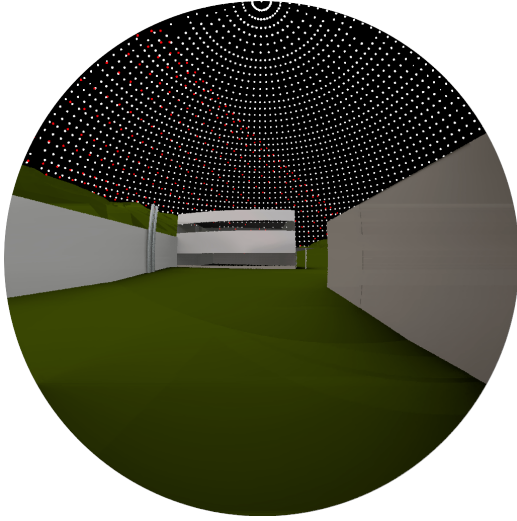


Figure 7: white: 5185 sun positions in Radiance Scene; red: quarter hourly real sun positions; reflected sun positions are visible in glass surfaces.

the shading state matrix for each sensor point is

$$\dim(s) = j_{max} \times k_{max}. \quad (2)$$

For  $n$  calculation points

$$\dim(C) = n \times j_{max}. \quad (3)$$

Summing over all  $C_j$  for one single point  $i$  gives:

$$\sum_{j=1}^{5185} C_j = \pi, \quad (4)$$

which is the integral over the projected hemisphere. If every  $C_{i,j}$  was divided by  $\pi$  they would represent dimensionless and relative contribution factors to a final illuminance. The final annual illuminance records are collected in matrix E:

$$\dim E = n \times k_{max} \quad (5)$$

### Sun-only in the Five-Phase Method

An update for equation (1) was presented with the Three-Phase and finally the Five-Phase Method in McNeil (2013). There the imperfection of sky discretization regarding direct solar contribution is reduced by modelling a sky that contains only sources of known solid angle at the centers of each of the 5185 Reinhart sky patches (illustrated in Figure 7). The sun at about  $1.5 \cdot 10^8$  km from the earth, with its radius of  $6.96 \cdot 10^5$  km has a mean half angle without atmospheric effect Blanc et al. (2013) of about:  $\delta_s = 0.266^\circ \pm 1.7\%$ . The 5185 solar disk positions in Figure 7 are used to determine the contribution  $C_{solar}$  of every disk to the illuminance on specified test points. The Reinhart 6x6 subdivision of the Trengenza sky discretization results in patches of about  $2^\circ \times 2^\circ$  to  $3.3^\circ \times 2^\circ$ . For an approximated, geocentric

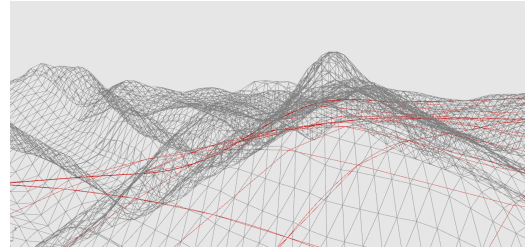


Figure 8: Errors by draping commands.

$180^\circ$  per 12 hour movement the sun's residence time in one patch is more than 8 minutes. This residence time varies throughout the year as angular velocity of the sun is not constant in respect to a geostationary coordinate system. This means, that the solar disk factors  $C_{solar}$  discretize real solar movements in at least 8 minute intervals. Atmospheric scattering effects let appear the sun even bigger. In Blanc et al. (2014) circumsolar scatter angles up to  $5^\circ$  are pointed out to contribute relevantly to solar applications. This scattering reduces the shortcomings of the otherwise defining 8 minutes of movement discretization in solar automation.

The Five-Phase method generates transfer coefficients for solar disks but uses the 5185 discretized sky patches as description in annual simulation. One coefficient for one single solar disk is multiplied by a discretized patch luminance, where luminance is spread over the full patch.

Latest implementations in Radiance use photon mapping algorithms. In Yang et al. (2013) this methodology was used to investigate environmental effects of solar concentrating facades.

### Digital Elevation and Buildings Models

Digitalization of the building construction sector leads to widely spread digital elevation and city models, which are available for input to the Radiance scenes. Highly resolved digital elevation models (DEM) contribute tens of thousands of surfaces to the Radiance scene and thus increase computation times to an unhandy extent. Reducing the number of surfaces by draping methods in different CAD systems is inappropriate because of peak smoothing. An example is illustrated in Figure 8. In this area of Figure 8, false draping would smooth most of mountain heights and by this, allow sun to reach buildings also on December 21<sup>st</sup> in the simulation model, when sun is blocked by mountains in real world. In this work the local authority's 10x10 m elevation data is interpreted by a Grasshopper script by Blickfeld7.com (2016).

Three dimensional city models are today available as cityGML including metadata such as e.g. textures or qualitative building description for building information modelling BIM projects. Examples are shown in Kolbe et al. (2012), Bremer et al. (2016) for solar potential modelling and Grebe (2013) for city of Berlin.

3D design of new buildings is a standard routine. Within the Building Information Modelling (BIM) design philosophy exporting models in standardized data format (e.g. IFC) is established. Hence, the target building and its urban surrounding buildings are available as 3D geometries. Though, if surface descriptions which are necessary for raytracing are missing, their definition is still manual workload for the simulation.

Particular attention in modelling elevation and building's data has to be paid due to different cartographic systems, and differences up to some tens of meters between ellipsoidal and geoidal heights.

### Implementation

Digital elevation models and digital building/city models are combined and used in the sun-only phase of the Five-Phase method to generate transfer (day-light) coefficient matrices  $C_{i,j}$  using Radiance *rcontrib* program.

```
rcontrib < points.txt -n 6 -I -ab 0 -ad 1 \\
-lw 0 -dc 1 -dt 0 -dj 0 -dp 0 -faa -e MF:6 \\
-f reinhart.cal -b rbin -bn Nrbins \\
-m solar scene.oct >> C.dsmx
```

The separation of state 1 and 2 is realized by changing the surface descriptions. This gives two different coefficient matrices (Figure 9):

- $C_{sr0}$  ... no solar reflection; all surfaces are black in the scene description
- $C_{sr1}$  ... one solar reflection; in the scene description all surfaces except windows and specular metal surfaces are blackened. Windows and metals are modeled as Radiance mirror material.

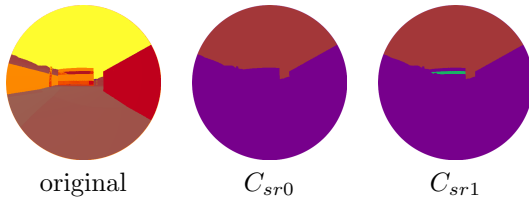


Figure 9: Different scene descriptions for the generation of the coefficient matrices with the *rcontrib* command.

For the coefficient pre-calculation a virtual sun-only *DAYSIM* weather file is generated and put into the work flow of Figure 10:

```
place Abfaltersbach
latitude 45.754668
longitude -12.523695
time_zone -15
site_elevation 900
weather_data_file_units 1
1 1 7.000000 800 1
1 1 7.250000 800 1
1 1 7.500000 800 1
1 1 7.750000 800 1
1 1 8.000000 800 1
```

This file is then input to *gendaymtx* routine:

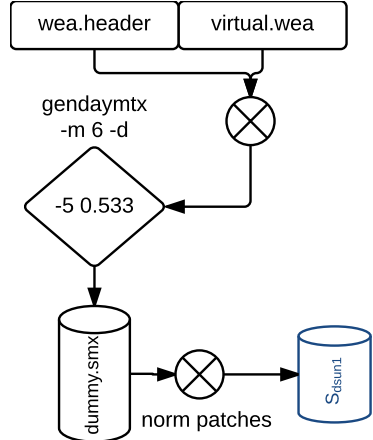


Figure 10: Generation of sky description  $s$ .

```
gendaymtx -5 0.533 -m -d virtual.wea > \\
dummy.smx
```

The number of time steps  $k_{max}$  in the dummy *DAYSIM* weather file shows quarter hourly resolution. For each time step the solar position is calculated according to a rudimentary algorithm in Radiance's *gensky* program, whose accuracy is limited compared to todays most advanced Solar Position Algorithm (SPA) in Figure 18. By applying command *-m 6* to *gendaymtx*, the sky division gives 5185 sky patches, *-d* gives no diffuse sky radiance and by *-5 0.533* the sun is not spread over three neighboring patches and solid angle discrepancy between solar disk and patch is compensated. So, the sky description  $s_k$  for one time step contains only one single entry, which is finally standardized to the reciprocal of its solid angle  $L_i = \frac{1}{\Omega_{i,\text{projected}}}$ . By this, the product of all visible solar disks and the corresponding standardized solar luminance will result in 1, but entries in  $S$  will no longer have physical meaning. The annual sky description is generated as shown in Figure 10 resulting in  $s_{dsun1}$ , where  $dsun1$  stands for "direct sun in one single patch". Radiance is providing 3 channels, which could be interpreted as RGB values. Therefore, the vector  $s_{dsun1}$  has  $k_{max}$  times three columns and 5185 lines. The product - using Radiance's *dctimestep* or *rtmxop* to collect the three Radiance channels - of the above described artificial annual skyvector  $s_{dsun1}$  and the transfer coefficients  $C_{*, i,j}$  is:

- $\tilde{S}_0 = C_{sr0} \cdot s_{dsun1}$ , showing no bounce insolation
- $\tilde{S}_1 = C_{sr1} \cdot s_{dsun1}$  showing no and one bounce insolation

$\tilde{S}_{1b}$ , thus describes only one bounce reflections.

$$\tilde{S}_{1b} = \tilde{S}_1 - \tilde{S}_0 \quad (6)$$

All data in  $\tilde{S}_*$  lack physical meaning and are translated into "0, 1 or 2"

- if  $\tilde{S}_{0,k} \neq 0 \rightarrow S_{0,k} \equiv 2$ ,

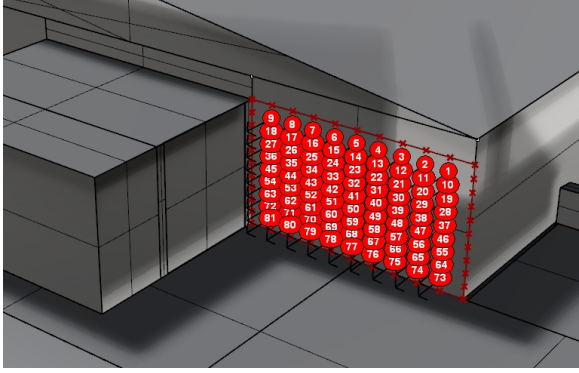


Figure 11: Point indices on test facade.

- if  $\tilde{S}_{1b} \neq 0 \rightarrow S_{1b} \equiv 1$ .

Finally

$$S = S_0 + S_{1b} \quad (7)$$

$$\dim S = n \times k_{max} \quad (8)$$

The definition of target points and surface normals on any facade (e.g. Figure 11) is automated within Software *Rhinoceros* using a *Grasshopper* script.

## Discussion and result analysis

### Case Study

Radiance's *rcontrib* raytracing on topography and building models delivers  $\{0, 1, 2\}$  data in matrix  $S$ . The approach was implemented and applied in a case study within a mountainous region (Figure 12). 81 test points were spread over the west facing facade, Figure 11.

The view from the office behind this facade is shown in Figure 13 for May 8<sup>th</sup> at 06:30am. The vis-a-vis facade is facing east and is partly glazed on two stores. At this time of year and day, the east facade is reflecting the morning sun onto the 81 test points on the west facade. This is clearly reproduced in our results for point 41 in Figure 16. Point 41 is approximately corresponding to the focal point of the camera in Figure 13. Between 6:00 and 7:00am, data shows state 1, insolated via reflection. From 11am to 6:30pm, the west facade is hit by direct insolation, state 2. Data for all points on the west facade is illustrated in Figure 14: When sun elevation is increasing, the points from top (low indices) to bottom (high indexes) are hit. At around 11:30am, the sun is directly visible from all 81 test points, and towards dusk the shadow



Figure 12: Panorama view of case study.

edge starts to move over the 81 points, resulting in the saw tooth structure in Figure 14. For easing understanding, point with index 0 is modelled horizontally on the roof, so it is hit by direct sun all day long.

Two main results are:

1. Missing vegetation in digital elevation models significantly affects the detection of states 0 and 2 for buildings that are particularly close to natural obstructions such as wooded hills (e.g. trees on hills in Figure 15).
2. The result for specific test day (Figure 16) shows the detection of state 1 between 6am and 7am. The real observation at 06:30am from viewpoint 41 is shown in Figure 13. This gives evidence that the concept works.

### Limitations

The pre-calculation of insolation states requires continuous updates in case of constructional activities nearby. It also cannot detect short-term mutations of the surrounding such as reflections from parked car. Seasonal changes caused by deciduous trees could be detected by creating two different matrices  $S$ . But this calls for an active switching between  $S_{leaves}$  and  $S_{no-leaves}$  in the shading control system by the Facility Management in spring and autumn.

Tilttable windows on nearby buildings are critical as long as their different surface normals are not modelled within the simulation and their current state is not detected. This could be solved using electromagnetic contacts and sending their signal to the shading automation.

The presented approach is not designed to consider glare evaluation metrics for viewpoints inside the building. It elaborates insolation states for facades. The location of the source of reflection is not detected by this approach, thus the louver system cannot be positioned to a tilt angle depending on the path of rays. But it can block rays from the full bottom quarter space by moving to a tilt angle of about 42° for a 80mm wide, 72mm spaced louver system.

The discretization of sun position works fine for planar surface. The modeling of any non-planar surfaces is difficult as surface triangulation eliminates



Figure 13: Insolation via reflection (state 1) on May, 8<sup>th</sup> 06:30am.

Matrix S: May 5th - 11th from 05-19

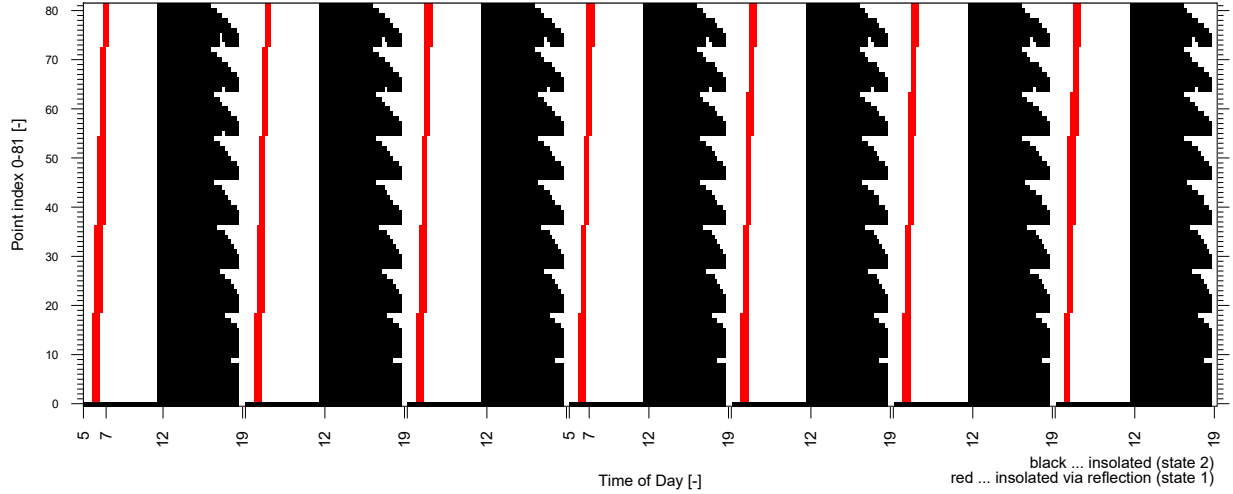


Figure 14:  $S$  for May 8th  $\pm$  three days.



Figure 15: Nearby wooded hills.

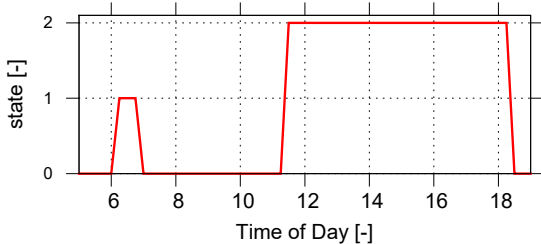


Figure 16: State detection for point 41.

adequate surface normal vectors.

The transfer coefficients are calculated for a set of 5185 sun positions. They are—set at the centers of Reinhart 6x6 sky patches—located on a  $\sim 2^\circ$  grid. This means, that this approach considers one specific shadow line for  $\sim 1^\circ$  off the discretized sun position, where real sun moves during a specified period  $\Delta t$  (Figure 17). The error of this discretization regarding the real shadow line on building facade cannot be generalized as the buildings mutual location is random and the shadow creating movement is related to the profile angle. These profile (=projected) angles are illustrated in Figure 17. Their velocity in  $^\circ$  per hour is depending on the facade orientation: for

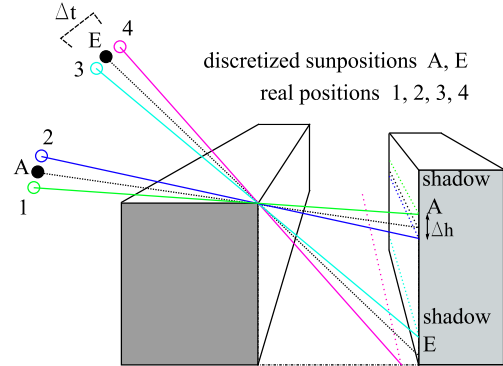


Figure 17: Discretized sun positions and temporal residence time.

example at a south facing facade there are two days every year (equinox), when the profile angle does not change throughout the day; or for a west facing facade, the profile angle varies from  $90^\circ$  to  $0$  within afternoon duration. In summary, the angular velocity (azimuthal, elevational, or profile angle) is depending on facade orientation and geographic position.

The calculation of the solar position is based on the Radiance *gensky* program. The difference between SPA and the *gensky* routine is about  $[-0.4^\circ, 0.48^\circ]$  and  $[-0.2^\circ, 1^\circ]$  for elevation and azimuth angles, respectively. This is a well-known inaccuracy of *gensky* and needs to be considered in accuracy definitions together with the inherent discretization inaccuracy of Figure 17.

## Conclusion

Solar shading automation will be accepted if its reactions to varying outdoor conditions are understandable. Today's practice can hardly identify if a win-

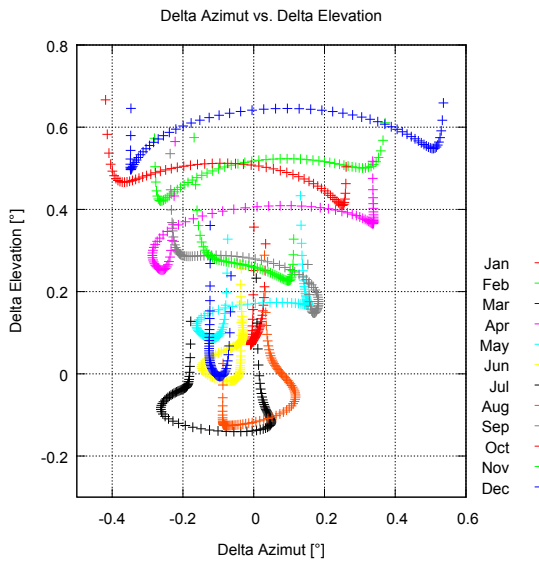


Figure 18: x: Azimuthal, y: Elevational difference between SPA and gensky solar positioning algorithm for each month 15<sup>th</sup> at location 45,75°N, 12,52°E.

dow is directly insolated (state 2), hit by a reflected sun beam (state 1) or shaded (state 0) by nearby structures and contours. The detection of these three states for every single contributing facade position is an essential part for comprehensible control of louver systems. This work uses raytracing techniques in annual daylight simulations to determine the insolation states per time step for all points of interest. Application in a case study shows that this approach provides good reproduction of reflected beam and direct insolation. The accuracy of digital elevation and building models is sufficient so that shadowing by buildings/topography and direct insolation is clearly reproduced. Today's automation shortcoming of non-detection of insolation via reflection can be solved by this approach, which is ready to be implemented into shading controls on the market.

## Acknowledgment

This work was supported by Austrian Funding Agency ffg in program "Stadt der Zukunft 1. Ausschreibung" under project number 845192.

## Nomenclature

### Glossary

**BIM** Building Information Modelling 3

**CAD** Computer Aided Design 3

**CIE 1994** Commission Internationale de l'Eclairage 2

**cityGML** City Geographic Markup Language 3

**DEM** Digital Elevation Model 3

**IFC** Industrial Foundation Classes 3

**SPA** Solar Position Algorithm 4, 6

## References

- Blanc, P., B. Espinar, N. Geuder, C. Gueymard, R. Meyer, R. Pitz-Paal, B. Reinhardt, D. Renné, M. Sengupta, L. Wald, and S. Wilbert (2014). Direct normal irradiance related definitions and applications: The circumsolar issue. *Solar Energy* 110, 561–577.
- Blanc, P., B. Espinar, and L. Wald (2013). Report on direct normal irradiance standards MACC-II. Technical report, 7th framework EC; 283576.
- Blickfeld7.com (2016). DTM DigitalTerrainMesh. [www.blickfeld7.com](http://www.blickfeld7.com).
- Borisenkov, E., R. Kittler, D. Kendrick, J. Krochmann, P. Littlefair, R. McCluney, J. Michalsky, H. Nakamura, M. Navvab, E. Ne'eman, R. Perez, N. Ruck, S. Secker, P. Tregenza, and P. Valko (1994). Cie 108-1994.
- Bourgeois, D., C. Reinhart, and G. Ward (2008). A Standards Daylight Coefficient Model For Dynamic Daylighting Simulations. *Building Research and Information* 36(1), 1–56.
- Bremer, M., A. Mayr, V. Wichmann, K. Schmidtner, and M. Rutzinger (2016). A new multi-scale 3D-GIS-approach for the assessment and dissemination of solar income of digital city models. *Computers, Environment and Urban Systems* 57, 144–154.
- Grebe, S. (2013). Eintritt in Phase 3 - virtualcitySYSTEMS. *Business Geomatics* (5/13).
- Kolbe, T. H., G. Grger, and C. Rnsdorf (2012). CityGML - Virtual 3D City Models.
- McNeil, A. (2013). The five-phase method for simulating complex fenestration with radiance. [www.radiance-online.org](http://www.radiance-online.org).
- Tregenza, P. (1987). Subdivision of the sky hemisphere for luminance measurements. *Lighting Research & Technology* 19(1), 13–14.
- Ward, G., R. Mistrick, E. Lee, A. Mcneil, and J. Jonsson (2011). Simulating the Daylight Performance of Complex Fenestration Systems Using Bidirectional Scattering Distribution Functions within Radiance. *LEUKOS* 7(4), 241–261.
- Weitlaner, R., W. Pohl, D. Geisler-Moroder, M. Werner, C. Mai, and R. Müller (2013). Entwicklung einer integralen Steuerung für Tages- und Kunstlicht unter Berücksichtigung energetischer Effizienz. In *Licht 2014*, 2014. LiTG.
- Yang, X., L. Grobe, and W. Stephen (2013). Simulation of Reflected Daylight from Building Envelopes. In *13th Conference of International Building Performance Simulation Association*, pp. 3673–3680.